



Facile synthesis and comparative study of the enhanced photocatalytic degradation of two selected dyes by TiO₂-g-C₃N₄ composite

Asma A. Alothman¹ · Asif Ayub² · Safa K. Hachim³ · Borhan Mustafa Mohammed⁴ · Farhat Hussain⁵ · Muhammad Altaf⁵ · Zainab Jawad Kadhim⁶ · Holya A. Lafta⁷ · Yasir S. Alnassar⁸ · Marwah A. Shams⁹ · Nada A. Almuhou¹ · Mohamed Ouladsmene¹ · Mika Sillanpaa¹⁰

Received: 11 August 2022 / Accepted: 14 December 2022 / Published online: 26 December 2022
© The Author(s), under exclusive licence to Springer-Verlag GmbH Germany, part of Springer Nature 2022

Abstract

Photocatalysis is considered a useful technique employed for the dye degradation through solar light, visible or UV light irradiation. In this study, TiO₂, g-C₃N₄, and TiO₂-g-C₃N₄ nanocomposites were successfully synthesized and studied for their ability to degrade Rhodamine B (RhB) and Reactive Orange 16 (RO-16), when exposed to visible light. The analytical techniques including XRD, TEM, SEM, DRS, BET, XPS, and fluorescence spectroscopy were used to explore the characteristics of all the prepared semiconductors. The photocatalytic performance of synthesized materials has been tested against both the selected dyes, and various experimental parameters were studied. The experimental results demonstrate that, in comparison to other fabricated composites, the TiO₂-g-C₃N₄ composite with the optimal weight ratio of g-C₃N₄ (15 wt%) to TiO₂ has shown outstanding degrading efficiency against RhB (89.62%) and RO-16 (97.20%). The degradation experiments were carried out at optimal conditions such as a catalyst load of 0.07 g, a dye concentration of 50 ppm, and a temperature of 50 °C at neutral pH in 90 min. In comparison to pure TiO₂ and g-C₃N₄, the TiO₂-g-C₃N₄, a semiconductor, has shown higher degradation efficiency due to its large surface area and decreased electron–hole recombination. The scavenger study gave an idea about the primary active species (·OH radicals), responsible for dye degradation. The reusability of TiO₂-g-C₃N₄ was also examined in order to assess the composite sustainability.

Keywords Composite · Dye degradation · Photocatalysis · TiO₂-g-C₃N₄

Introduction

Water pollution is now considered a major concern globally. A large number of pollutants of different natures and compositions from various sources such as industries including

pharmaceutical, leather, textile, dyeing, and paper discharged untreated into the water system (Ayub et al. 2022). The improvement in textile industries has demanded more production of chemical dyes for dyeing purposes, resulting in major environmental threats, particularly in third-world countries. These dyes are chemically stable compounds and

Responsible Editor: Sami Rtimi

✉ Asif Ayub
asif.chemist45@gmail.com

¹ Department of Chemistry, College of Science, King Saud University, Riyadh 11451, Saudi Arabia

² Institute of Chemistry, The Islamia University of Bahawalpur, Bahawalpur 63100, Pakistan

³ Medical Laboratory Techniques Department, Al-Farahidi University, Baghdad, Iraq

⁴ Engineering Department, Mazaya University College, Nasiriyah, Dhi Qar, Iraq

⁵ Department of Chemistry, Government College University Faisalabad, Faisalabad 38000, Pakistan

⁶ Optics Techniques Department, Al-Mustaqbal University College, Hillah, Iraq

⁷ Al-Nisour University College, Baghdad, Iraq

⁸ The University of Mashreq, Baghdad, Iraq

⁹ Technical Engineering College, Al-Ayen University, Nasiriyah, Thi-Qar, Iraq

¹⁰ Department of Biological and Chemical Engineering, Aarhus University, Norrebrogade 44, 8000 Aarhus C, Denmark

non-biodegradable pollutants. Organic dyes are carcinogenic and may cause harmful effects on human health. So, these pollutants must be eradicated from aqueous systems before use (de Assis et al. 2021)(Ayub and Raza 2021).

Several techniques such as physical (sedimentation, filtration, and adsorption), biological (aerobic and anaerobic treatments), acoustical (radiation and electric processes), and chemical methods (electrochemical oxidations, oxidation, coagulation, and advanced oxidation processes) have been employed for treatment of polluted water (Ayub et al. 2020). Nowadays, advanced oxidation processes (AOPs) are becoming popular for the treatment of dye-contaminated water and the degradation and disinfection of various pollutants. These processes are very efficient for the eradication of industrial organic pollutants (Saeed et al. 2022).

In recent years, the photocatalytic technique via semiconductors is becoming popular among researchers, due to its low cost, high efficiency, and reusability, for the degradation of organic contaminants. In the past few years, there has been a lot of research on the use of photocatalysis for wastewater treatment. It is thought to be an advanced, ecologically acceptable alternative technology for the degradation of organic contaminants. Compared to other conventional physical and biological methods, it has low-cost and simple operational properties (Moustafa et al. 2022).

In the photocatalytic process, electron–hole pairs generate in CB and VB of the photocatalysts under light irradiation. These photogenerated excitons help in the degradation of dyes and industrial pollutants. ZnO, CdS, CuO, V₂O₅, TiO₂, and many other semiconductor photocatalysts are now being tested for dye degradation (Yu et al. 2022). Among different semiconductor photocatalysts, TiO₂ has been proven an effective catalyst due to its positive features like higher oxidizing power, photocatalytic performance, cost-effectiveness, low toxicity, and chemical stability (Pattanayak et al. 2022). A large band gap of TiO₂ of 3.20 eV decreases its photocatalytic activity under solar light, but it is a very effective photocatalyst under UV light (Camposeco and Zanella 2022).

The g-C₃N₄ has gained the attention of the researcher because of its merits like facile synthesis, low toxicity, and cost efficiency which make it a good candidate for the degradation of some natural organic dyes. It is chemically stable under strongly acidic and basic conditions (Waghchaure et al. 2022). However, a low band gap and fast recombination of holes and electrons limit its performance for photocatalytic activity. Various techniques such as doping with metal oxides, coupling with semiconductors, and non-metallic elements have been applied to increase its catalytic ability. Coupling of g-C₃N₄ with inorganic semiconductors such as metal oxide is a useful method that retards the above-mentioned drawback and improves the catalytic activity of g-C₃N₄. The combination of g-C₃N₄ with TiO₂ develops a heterojunction which helps in reducing the band gap of

metal oxides effectively and separating the charge carriers (Pattanayak et al. 2022).

In the current study, series of TiO₂-g-C₃N₄ nanocomposites have been fabricated and their dye degrading efficiency was investigated against two organic dyes i.e., RhB and RO-16. The purpose of this study was to fabricate environment friendly as well as cost-effective nanocomposites for the photodegrading of both dyes. The mechanism of photochemical degradation of dyes has been discussed in detail. BET surface area and fluorescence analyses were used to provide a potential reason for higher photocatalytic efficiency. To evaluate the sustainability of the semiconductor, the reusability of the composite has also been investigated for five cycles.

Experimental section

Reagents

All chemicals used in this study including tetrabutyl titanate Ti(OBu)₄, methanol (CH₃OH), ethanol (CH₃CH₂OH), melanine, nitric acid (HNO₃), sulfuric acid (H₂SO₄), isopropyl alcohol (IPA), p-benzoquinone (p-BQ), silver nitrate (AgNO₃), and ammonium oxalate (AO); RhB and RO-16 were purchased from Merk Ltd. Double-distilled water was used throughout the study.

Synthesis of photocatalysts

Synthesis of TiO₂ nanoparticles

The TiO₂ NPs were prepared by hydrothermal process (Zada et al. 2018). Briefly, 10 mL of Ti(OBu)₄ was mixed in 10 mL of ethanol while the mixture was stirred continuously. This mixture was poured into another solution mixture, having ethanol (40 mL), water (10 mL), and HNO₃ (2 mL) under stirring conditions. The resultant solution mixture underwent a hydrothermal reaction by transferring to an autoclave and heating it at 160 °C for 6 h. After that, the autoclave was cooled to room temperature.

The product was washed with deionized water (DW) for 10 times and then dried at 80 °C; the dried material was then calcined at 450 °C for 2 h to fabricate TiO₂ NPs.

Synthesis of g-C₃N₄ nanosheets

By using a chemical exfoliation process, the g-C₃N₄ nanosheets were fabricated (Raziq et al. 2015). A desired dose of the C₃N₄ was calcined at 500 °C in a muffle furnace for 4 h. Then, 3 g of the calcined C₃N₄ was dissolved in sulfuric acid (40 mL) under vigorous conditions for 48 h.

This solution mixture was added to a flask with 400 mL of distilled water and subjected to ultrasonic treatment for 12 h. The solution's dark color was changed to pale yellow. After centrifuging the resulting suspension, any leftover acid was thoroughly removed using DW and then dried at 80 °C. For the removal of structural defects, the synthesized, dried powder of C_3N_4 was added to 500 mL of methanol and heated at 65 °C for 12 h. In the final step, the suspension was centrifuged and dried at 100 °C, yielding g- C_3N_4 nanosheets.

Synthesis of TiO_2 -g- C_3N_4 nanocomposite

To synthesize different TiO_2 -g- C_3N_4 nanocomposites, 15 mg ground powder of prepared g- C_3N_4 was added to 50 mL of methanol and 10 mL of water. 100 mg of TiO_2 NPs was dispersed into the above-prepared solution mixture and stirred overnight. The residual methanol was evaporated by heating in a water bath and a grey solid material was obtained and dried under a vacuum condition at 70 °C. Finally, the material was calcined at 500 °C for 2 h in a muffle furnace (Ma et al. 2018). Based on the above-described method, several TiO_2 -g- C_3N_4 nanocomposites were synthesized. The mass ratio of g- C_3N_4 to TiO_2 was 0.00, 0.03, 0.10, and 0.15, and resultant composites were labeled as TCN-0 (pure TiO_2), TCN-03, TCN-10, and TCN-15, respectively.

Characterization

The XRD technique was used to evaluate the crystalline phase of the prepared catalysts. The XRD spectra were recorded on an X-ray diffractometer (Bruker D8, Germany) with $Cu\ \alpha$ radiation and operated at 40 kV. Fluorescence spectra of photocatalysts were obtained by a fluorescence spectrometer (PerkinElmer LS55). The TEM and SEM images of prepared samples were captured with a JEOL JEM-2100 electrons microscope and a Hitachi S-4800 scanning electrons microscope, respectively. A spectrophotometer (Shimadzu, UV-2450) was used to obtain the DRS spectra of the samples. XPS spectra of the samples were recorded on a Perkin Emmer Phi 5000G ESG system at 250 W. All binding energies were referenced to the C 1 s peak at 284.6 eV.

Photocatalytic degradation experiments

The photocatalytic efficiency of TiO_2 , g- C_3N_4 , and all TCN nanocomposites was tested by photodegradation of RhB and RO-16 dyes under visible light irradiations. In a typical procedure, 50 mL solution (50 ppm) of target dyes (RhB and RO-16) was poured into separate beakers and the desired amount of photocatalyst was added to the dye solutions. Reaction mixtures were placed on a hot plate to maintain

a temperature of 40 °C and were stirred for 90 min under visible light irradiations. To achieve equilibrium, the reaction mixture was stirred for 30 min under dark conditions. A small amount of samples were taken out of the reaction mixture at regular intervals of 15, 30, 45, 60, 75, and 90 min and were analyzed with a UV–visible spectrophotometer (JASCOV-570 spectrophotometer). The absorbance of every sample was noted. The percentage degradation of RhB and RO-16 was calculated using Eq. (1):

$$\text{Degradation \%} = \frac{[A]_0 - [A]_t}{[A]_0} \times 100 \quad (1)$$

where $[A]_0$ is the absorbance at zero minute and $[A]_t$ is the absorbance at various time intervals.

The above experiments were also carried out in the presence of scavengers to better understand the mechanism and recognize the reactive species in the photocatalytic processes. IPA, p-BQ, $AgNO_3$, and AO were specifically used as $\cdot OH$, $O_2\cdot^-$, e^- , and h^+ quenchers, respectively. Additionally, 5 cycles of repetition were carried out to evaluate the stability and reusability of the photocatalyst.

Results and discussion

X-ray diffraction

The pure g- C_3N_4 , TiO_2 , TCN-03, TCN-10, and TCN-15 composites have been analyzed by XRD as shown in Fig. 1, to evaluate the phase composition and any change in the crystal structure of the composite material. For pure g- C_3N_4 , two prominent peaks at 2θ of 13.2° and 27.4° were detected,

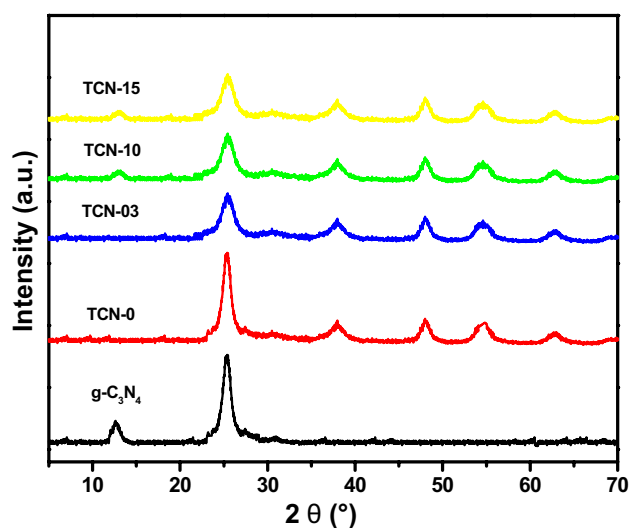


Fig. 1 X-ray diffraction patterns of g- C_3N_4 , TCN-0, TCN-03, TCN-10, and TCN-15

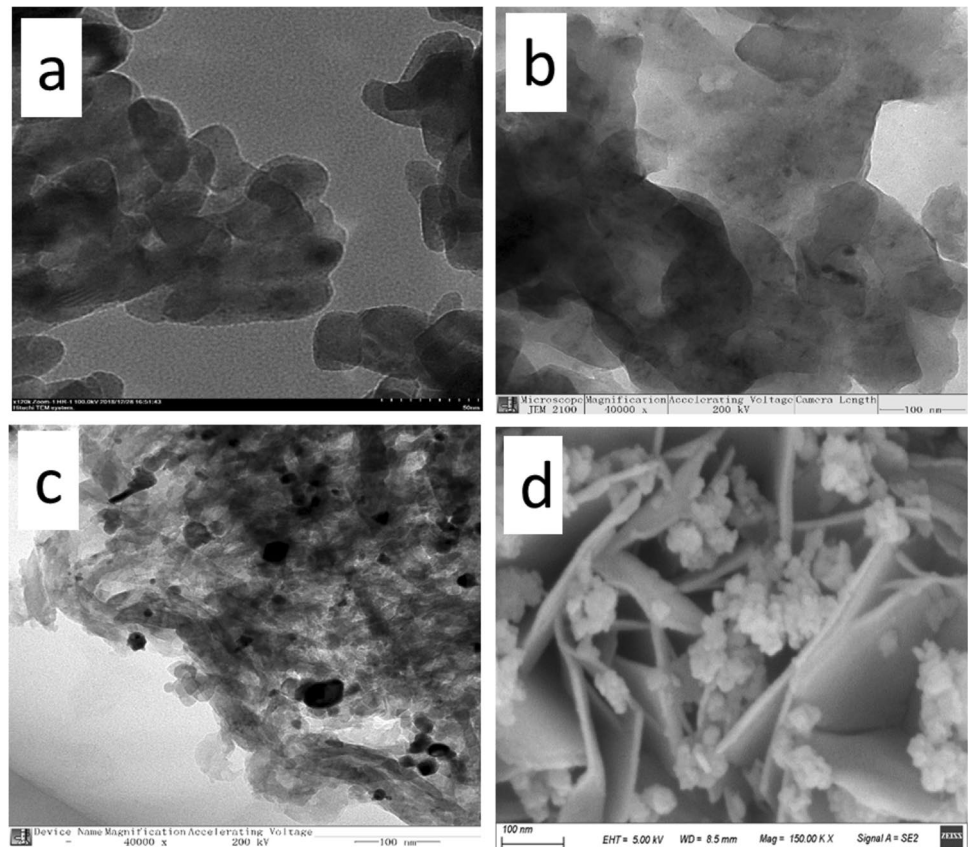
which were indexed to (100) and (002) plane diffractions of $g\text{-C}_3\text{N}_4$. For TiO_2 , peaks appearing at 25.4° , 37.7° , 48.2° , and 54.1° were indexed to (101), (004), (200), and (105) indicating the anatase phase TiO_2 (Gao et al. 2020).

Compared with pristine $g\text{-C}_3\text{N}_4$, all composite samples (TCN-03, TCN-10, and TCN-15) showed four additional peaks of TiO_2 appearing at 25.4° , 37.7° , 48.2° , and 54.1° which confirm the formation of composites. After $g\text{-C}_3\text{N}_4$ loading on TiO_2 , no peak of $g\text{-C}_3\text{N}_4$ was seen at 13.2° in sample TCN-03 which may be due to the low content of $g\text{-C}_3\text{N}_4$ and low crystallinity of the composite. But when the concentration of $g\text{-C}_3\text{N}_4$ was increased in the composites, both the characteristic peaks of $g\text{-C}_3\text{N}_4$ at angles 13.2° and 27.4° were observed in the other two composites (i.e., TCN-10 and TCN-15); this confirms the successful fabrication of composites. Careful observation reveals that the intensity of the main peaks of anatase titania slightly decreased by increasing the $g\text{-C}_3\text{N}_4$ content in the composites. The results of this study agree with the findings of Wang et al. (2022) in which they observed that the peaks for TiO_2 at 25.2° , 37.8° , 47.9° , 53.8° , 55.6° , and 62.7° correspond to (101), (004), (200), (105), (211), and (204), respectively, for the anatase TiO_2 .

Morphology

The morphology of $g\text{-C}_3\text{N}_4$, TiO_2 , and TCN-15 composites was analyzed by SEM and TEM studies. TEM analysis verified the formation of the TCN-15 composite. The prepared $g\text{-C}_3\text{N}_4$ shows a lamellar structure with wrinkles on the surface as shown in Fig. 2a (Wang et al. 2018). Figure 2b shows the TEM image of prepared TiO_2 which depicts the elongated spherical morphology. In the TEM image of TCN-15 (Fig. 2c), two different morphologies were observed, a grey sheet of $g\text{-C}_3\text{N}_4$ having a dark area because of TiO_2 particles and also showing a random covering of $g\text{-C}_3\text{N}_4$ layers with TiO_2 NPs. The TiO_2 NPs are incorporated on $g\text{-C}_3\text{N}_4$. Figure 2d shows the SEM image of the prepared TCN-15 composite. Nanosheets of $g\text{-C}_3\text{N}_4$ containing clusters of TiO_2 are obvious from SEM images. Agglomeration of particles of TiO_2 introduced roughness in the nanosheets of $g\text{-C}_3\text{N}_4$ and increased the degrading capacity of the composite. SEM analysis may also refer to the formation of heterojunction among the components of the prepared composite that increases the degradation efficiency of the composite (Kholikov et al. 2021).

Fig. 2 TEM images of **a** pure $g\text{-C}_3\text{N}_4$, **b** TCN-0, and **c** TCN-15. SEM image of **d** TCN-15



DRS analysis

Figure 3 shows the absorbance spectra of pure $g\text{-C}_3\text{N}_4$, TiO_2 , TCN-03, TCN-10, and TCN-15 composites to study their optical properties. Absorbance spectra of $g\text{-C}_3\text{N}_4$ as shown in Fig. 3a revealed that $g\text{-C}_3\text{N}_4$ photocatalyst show an absorbance edge at a higher wavelength of 465 nm, whereas TiO_2 at a shorter wavelength of 385 nm (Mehregan et al. 2022). All prepared composites such as TCN-03, TCN-10, and TCN-15 have shown absorbance at a higher wavelength of 413, 436, and 449 nm, respectively, when compared with pure TiO_2 . This shift in absorption edge toward higher wavelength was due to an increase in $g\text{-C}_3\text{N}_4$ contents in the composite series. So, the band gap of all the prepared composites decreased as compared to pure TiO_2 . Therefore, $\text{TiO}_2\text{-}g\text{-C}_3\text{N}_4$ shows better catalytic performance under visible light irradiation

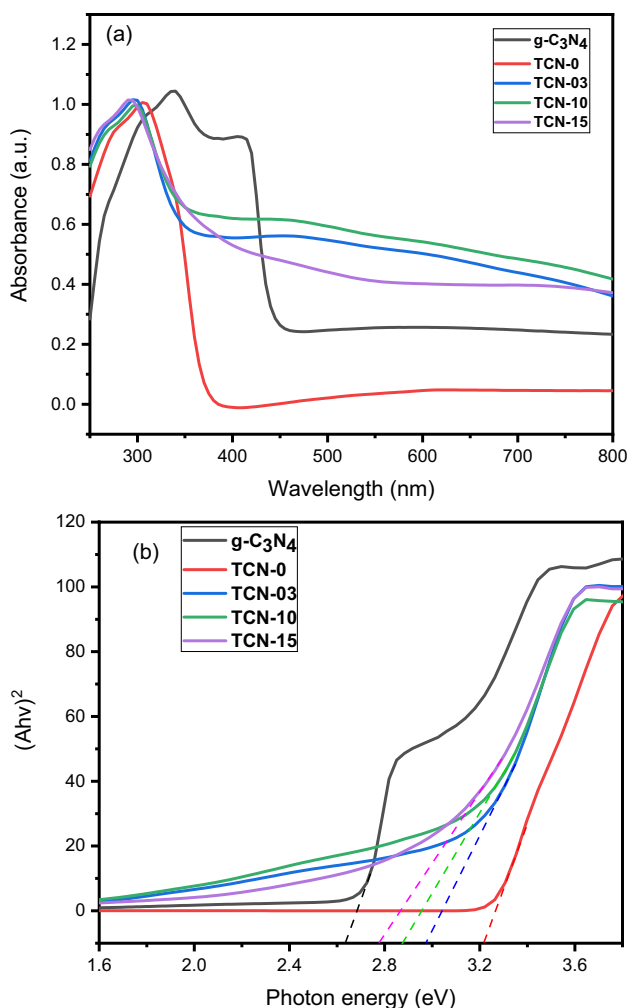


Fig. 3 a UV-vis absorbance spectra of $g\text{-C}_3\text{N}_4$, TCN-0, TCN-03, TCN-10, and TCN-15 and b Kubelka-Munk plot for the band gap determination

(Zhang et al. 2021). The Kubelka-Munk formula was used to calculate the band gap energy (E_g) of all the synthesized semiconductors. Plotting the square of the modified Kubelka-Munk function vs photon energy ($h\nu$) gives the optical band gap energy (E_g) of pure $g\text{-C}_3\text{N}_4$ (2.63 eV), TiO_2 (3.21 eV), TCN-03 (2.97 eV), TCN-10 (2.87 eV), and TCN-15 (2.78 eV) as shown in Fig. 3b.

Fluorescence spectroscopy

The amount of OH radicals generated was measured using the coumarin fluorescence technique since the generation of OH radicals is essential for photocatalysis. Because it readily generates luminous 7-hydroxy coumarin by interaction with OH radicals, coumarin is used in this technique. The signal intensity in the fluorescence spectrum will typically increase, as the quantity of OH radicals increases (Kotkar et al. 2022).

The fluorescence spectra of pure $g\text{-C}_3\text{N}_4$ and its composites with TiO_2 are shown in Fig. 4 in relation to the generated OH radicals. It is evident that when the quantity of $g\text{-C}_3\text{N}_4$ coupling increases, the OH radical fluorescence intensity of $\text{TiO}_2\text{-}g\text{-C}_3\text{N}_4$ becomes greater than that of pure $g\text{-C}_3\text{N}_4$, particularly in the case of a TCN-15 sample. Consequently, TCN-15 is regarded as a powerful photocatalyst for the elimination of contaminants (Adeel et al. 2021). Fluorescence spectra confirm the existence of $\cdot\text{OH}$ radicals which on the other hand confirms the successful synthesis of $\text{TiO}_2\text{-}g\text{-C}_3\text{N}_4$ composites.

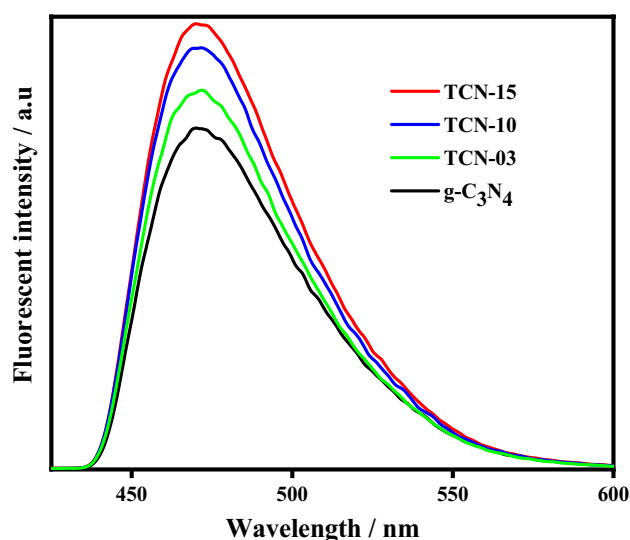


Fig. 4 Fluorescence spectrum of pure $g\text{-C}_3\text{N}_4$ and composites (TCN-03, TCN-10, TCN-15)

BET analysis

The BET analysis of prepared $g\text{-C}_3\text{N}_4$ and TCN-15 composite was performed to estimate the surface area and pore size distribution. In general, photocatalysts often having higher surface area and more reaction sites, exhibit higher adsorption capacity. Nitrogen adsorption/desorption isotherm was employed along with BET measurement to evaluate the porous structures of pure $g\text{-C}_3\text{N}_4$ and TCN-15 composite as shown in Fig. 5. The $g\text{-C}_3\text{N}_4$ and TCN-15 composites have type IV- H_3 hysteresis loops which represent the slit-shaped mesoporous (Ma et al. 2018). The BET surface area of the TCN-15 composite ($26.3 \text{ m}^2/\text{g}$) was larger than the pure $g\text{-C}_3\text{N}_4$ ($4.2 \text{ m}^2/\text{g}$). TCN-15 exhibit higher dye degrading efficiency compared to pure $g\text{-C}_3\text{N}_4$ which may be due to two possible reasons. First, the $g\text{-C}_3\text{N}_4$ has a smaller particle size and lower density; second, the $g\text{-C}_3\text{N}_4$ had high dispersion on the surface of microporous TiO_2 due to its ultrasonic

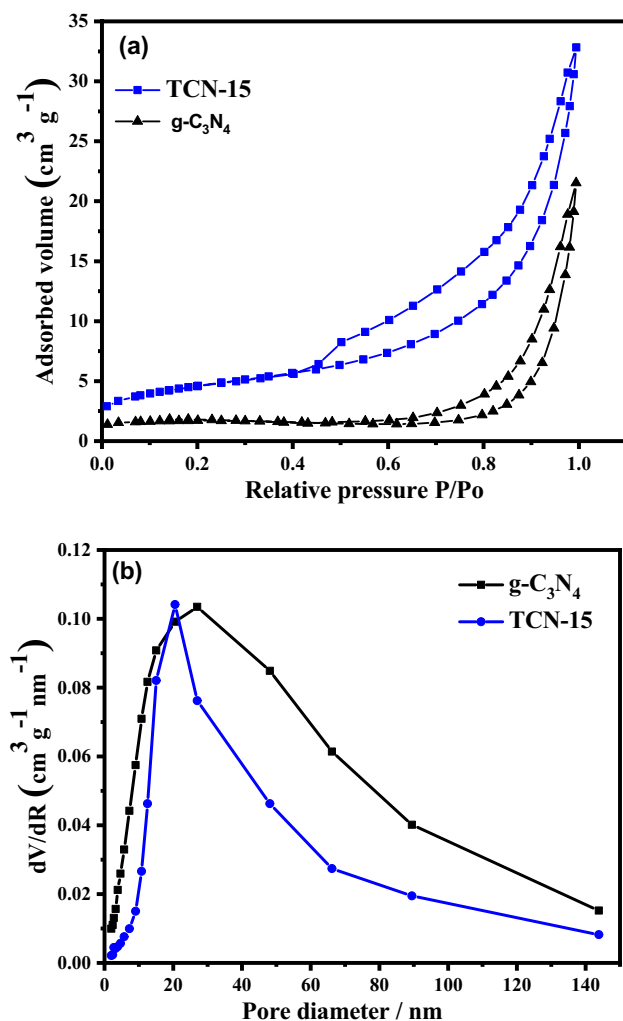


Fig. 5 **a** The N_2 adsorption–desorption isotherms and **b** pore size distribution plots of samples

treatment. Thus, the TCN-15 composite was utilized in the following study (Girish et al. 2022).

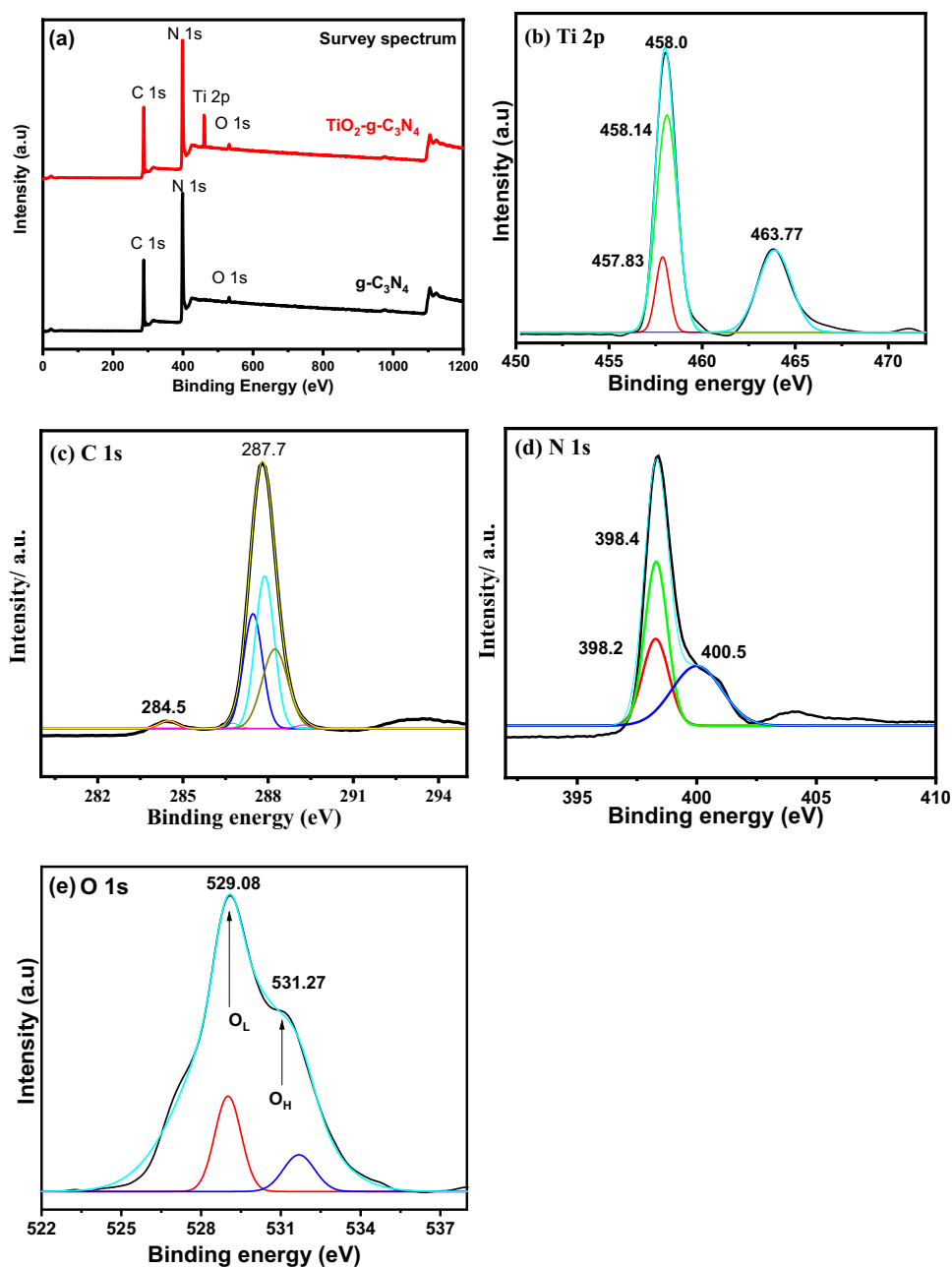
XPS analysis

The XPS spectrum of $g\text{-C}_3\text{N}_4$ and TCN-15 composite is shown in Fig. 6a, with the peak locations adjusted using C 1 s at 284.8 eV. The XPS survey spectra of $g\text{-C}_3\text{N}_4$ and TCN-15 composite show the presence of C, O, N, and Ti components which is consistent with their chemical formulae. The Ti 2p spectra of TCN-15 can be seen in Fig. 6b, and they exhibit two peaks having 458.7 (Ti 2p 3/2) and 463.7 eV, binding energies, respectively. The binding energies of Ti 2p in TCN-15 show the heterojunction structure among the precursors of the composite (Alsalmeh et al. 2022). The high-resolution spectra of C 1 s, N 1 s, and O 1 s, of TCN-15, have been shown in Fig. 6c–e. TCN-15 composites displayed an additional peak above 288.2 eV in addition to the C 1 s peak. A closer look revealed that the aromatic ring N–C = N₂ peak for TCN-15 was at 287.7 eV. The peaks at 398.2, 398.4, and 400.5 eV can be found in the N 1 s high-resolution spectra. The lattice Ti–O bond was thought to be responsible for the major peak at around 529.08 eV, while the hydroxyl (O–H) group was thought to be responsible for the minor peak at 531.27 eV (Liu et al. 2022). In general, the samples' photocatalytic capabilities are significantly influenced by the surface OH groups. The hydroxyl content was higher in TCN-15 as depicted in fluorescence spectra. The presence of additional hydroxyl groups on the catalysts' surfaces may help to capture holes before they reach the surface, improving charge-transfer efficiency and photocatalytic activity.

Photocatalytic performance

The dye-degrading properties of synthesized semiconductors were tested against RhB and RO-16 dyes under visible light irradiations. Figure 7 shows the different trends of the photocatalytic activities against both dyes. The $g\text{-C}_3\text{N}_4$ has shown 31.59% and 38.46% degradation efficiency for RhB and RO-16 respectively, while the degradation efficiency of TiO_2 against RhB and RO-16 was observed only 37.81% and 44.05% after 90 min. It was observed that all the prepared composites have shown higher photocatalytic performance compared with pure TiO_2 and $g\text{-C}_3\text{N}_4$ within 90 min under visible light. Among all the synthesized $\text{TiO}_2\text{-}g\text{-C}_3\text{N}_4$ composites, TCN-15 has shown the better photocatalytic degradation performance of 85.8% and 88.56% for RhB and RO-16 dyes respectively, in 90 min, while TCN-03 has shown the lowest degradation efficiency of 67.20% and 58.04% among all composites. TiO_2 absorbs in the UV region of light and high TiO_2 content in composite reduce the

Fig. 6 XPS survey spectra of a $g\text{-C}_3\text{N}_4$ and TCN-15. High-resolution XPS spectra of TCN-15: **b** Ti 2p, **c** C 1s, **d** N 1s, and **e** O 1s



catalytic ability of photocatalyst by blocking the visible light at the surface of $g\text{-C}_3\text{N}_4$. This may lower the rate of formation of photogenerated positive holes and electrons (Jeyaraja et al. 2022). Lesser formation of excitons in TCN-03 and TCN-10 composites having the highest amount of TiO_2 and less amount of $g\text{-C}_3\text{N}_4$ causes a decrease in photocatalytic performance (Kumar et al. 2022). Hence, the TCN-15 composite has shown better catalytic activity than pure TiO_2 , $g\text{-C}_3\text{N}_4$, and other nanocomposites. The OH radicals are responsible for the better catalytic activity of the TCN-15 composite as shown by the fluorescence study.

Effect of dosage

The photocatalytic performance of the TCN-15 composite was tested by degradation of RhB and RO-16 dye using different amounts of TCN-15 catalyst from 0.01 to 0.09 g/L in 50 mL (50 ppm) dye solution and conditions were maintained as temperature 40°C , at natural pH, under visible light irradiation for 90-min. It was observed that by a gradual increase in the quantity of TCN-15 composite from 0.01 g to 0.07 g/L the increase in the RhB degradation was observed from 79.2 to 87.10% as shown in Fig. 8a while 70.8% to 94.40% RO-16 degradation was

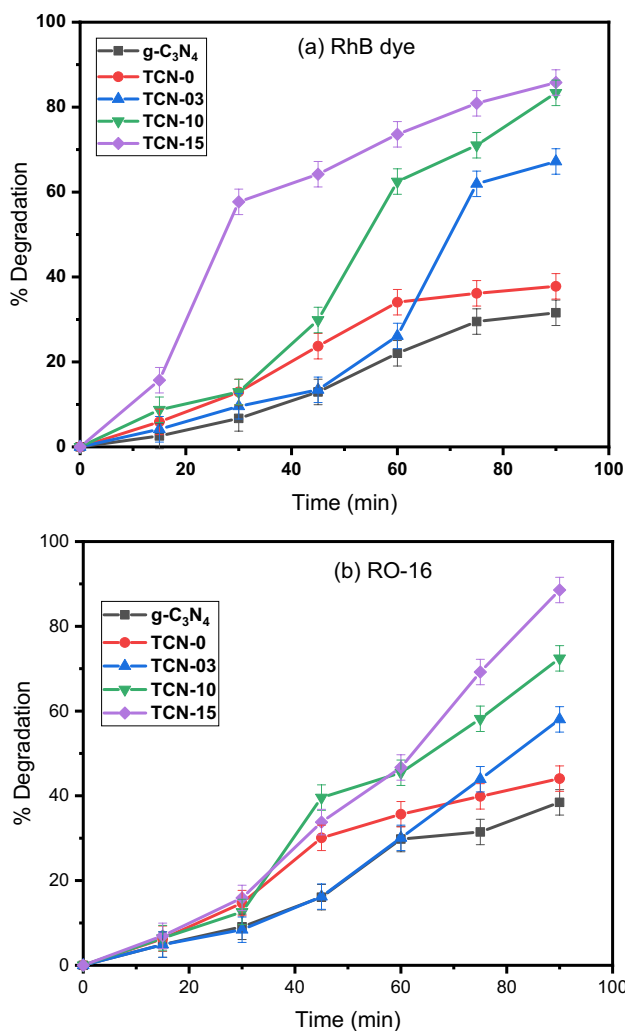


Fig. 7 Plot of percentage degradation of **a** RhB and **b** RO-16 with pure $g-C_3N_4$, TCN-0, TCN-03, TCN-10, and TCN-15

noticed at the same change in dose, shown in Fig. 8b. The percentage degradation increased by increasing the dosage of catalyst. After a certain limit, further increases in the dosage of the catalyst did not affect the catalytic efficiency. For both dyes, 0.07 g photocatalyst showed maximum degradation efficiency. The number of active sites increases with an increase in the dosage of the catalyst. However, the reaction mixture cannot be homogenized properly at a higher dosage of catalyst and high agitation, in this situation, the active sites of the composite were not fully available at a high dose concentration. The increase in the catalyst dose from 0.07 to 0.09 g results in a decrease in the photocatalytic activity from 87.10 to 83.3% and 94.40 to 85.3% for RhB and RO-16 dyes, respectively. Furthermore, the higher dose also blocks the penetration of light and may also affect the catalytic efficiency (Tara et al. 2021).

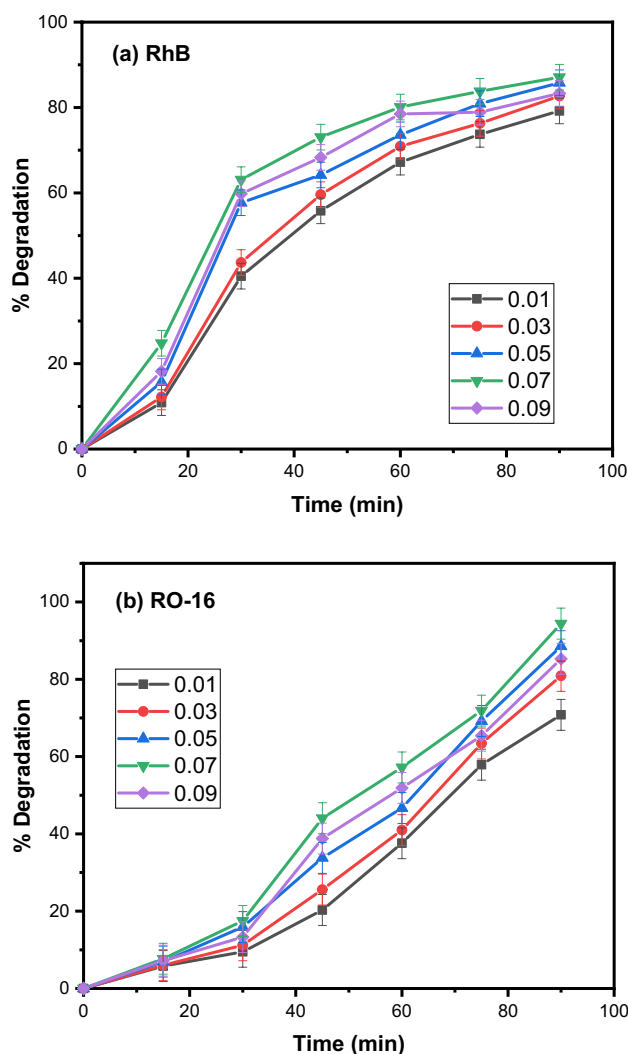


Fig. 8 Plot of percentage degradation of **a** RhB and **b** RO-16 at different catalyst doses of TCN-15

Effect of temperature

As temperature also affects the reaction rate, the dependence of dye degradation on temperature was investigated by performing photodegradation experiments with 0.07 g of TCN-15 in 50 mL of (50 ppm) RhB and RO-16 dye solution at 30, 40, and 50 °C separately, at natural pH under visible light irradiation for 90 min. Figure 9a and b show that the percentage degradation of both dyes increased with an increase in temperature. 80.08%, 87.10%, and 89.62% degradation was recorded for RhB, while for RO-16 dye, 78.8%, 94.4%, and 97.2% degradation was observed at 30, 40, and 50 °C, respectively. The enhanced catalytic activity of the TCN-15 composite at a higher temperature may be due to the higher kinetic energy of the substrate which increases the collision frequency. As a result, recombination of charge carriers is reduced which increases the catalytic activity of the TCN-15 composite (Adeel et al. 2021).

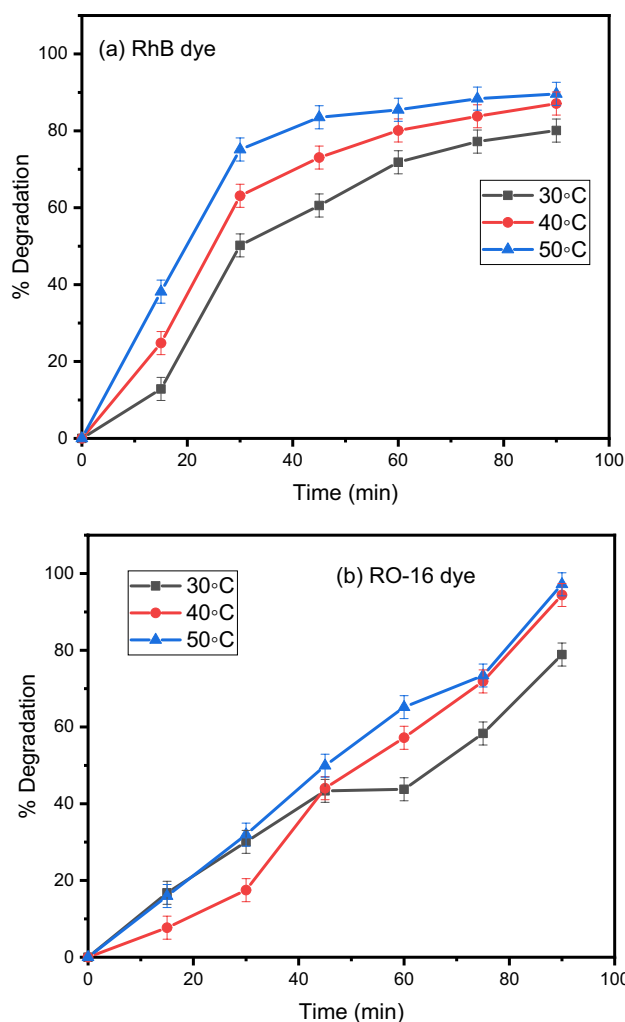


Fig. 9 Plot of percentage degradation of **a** RhB and **b** RO-16 at different temperatures with TCN-15

Effect of concentration

The effect of dye concentrations on the degradation efficiency of the photocatalyst was measured, and three degradation experiments were performed separately with 0.07 g of TCN-15 in 50 mL of (50 ppm) RhB and RO-16 dye solution by changing the concentration of dye solution from 50 to 150 ppm for the regular time interval from 0 to 90 min under visible light irradiation at natural pH and optimal conditions, the results have been presented in Fig. 10. The percentage degradation data showed that photocatalysts degraded 89.6, 83, and 75% of RhB dye, while 97.2, 85, and 66% of RO-16 dye in 50, 100, and 150 ppm dye solution in 90 min, respectively. It can be observed that the catalytic activity of TCN-15 composite decreases with an increase in dye concentration because more active sites of TCN-15 composite are covered and the light penetration is decreased (Sanakousar et al. 2022b). Furthermore, as all other factors

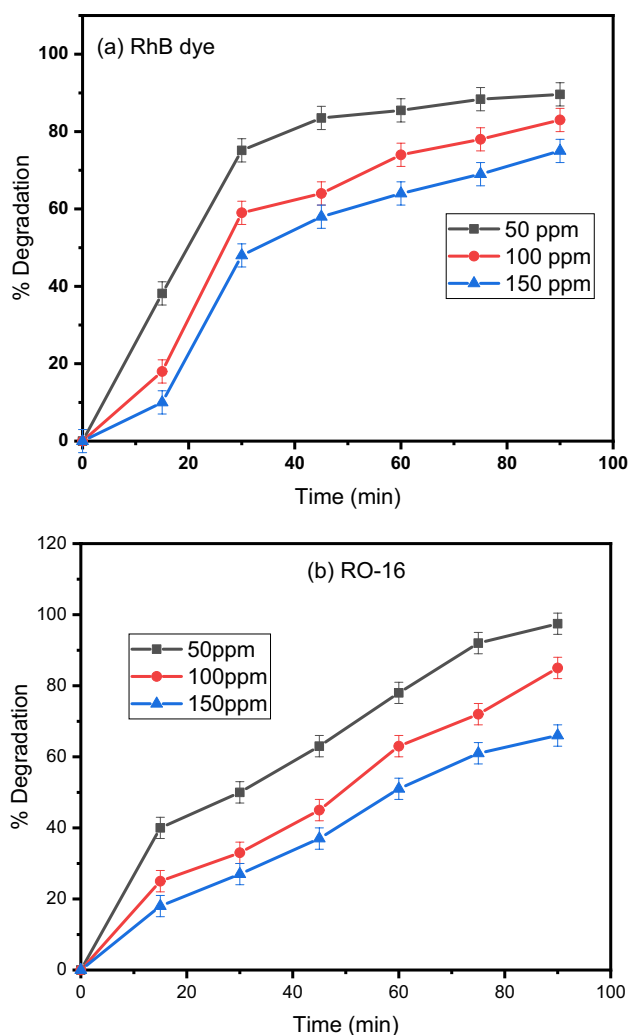


Fig. 10 Plot of percentage degradation of **a** RhB and **b** RO-16 at different dye concentrations with TCN-15

are constant, the relative concentration of OH radicals decreases. As a result, catalytic efficiency is decreased at higher concentrations.

Photocatalyst stability

The stability of the TCN-15 composite was evaluated by five degradation experiments. The concentration of RO-16 dyes and percentage degradation gave an insight into the degrading efficiency of the prepared composite. After each degrading experiment, the composite was washed with deionized water to remove the RO-16 dye adsorb on the surface and dried. Figure 11a shows that the TCN-15 composite was stable even after five cycles of regeneration and could retain 85.9% degrading efficiency. The decrease in the degrading efficiency may be due to the loss of composite due to washing (Sun et al. 2022). After five recycling experiments, the

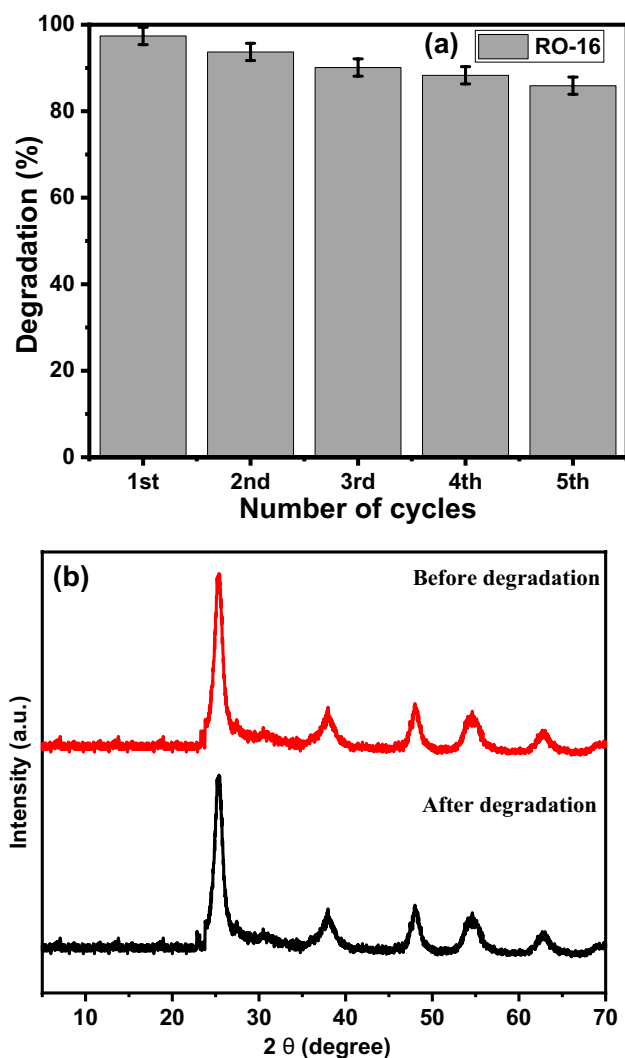


Fig. 11 a Photocatalytic stability of TCN-15 catalyst with RO-16 dye and b XRD spectrum of fresh and reused TCN-15 catalyst

remarkable photocatalytic stability of the TCN-15 composite catalyst was confirmed by the XRD pattern of the TCN-15 composite's fresh and reused samples indicating that the crystallinity and morphological properties remained the same (Fig. 11b).

Scavenger study

To find out the species responsible for the photodegradation of selected dyes such as RO-16, essential to clarify the degrading mechanism of TCN-15 composite, radical trapping experiments were performed. The system's $\cdot\text{OH}$, $\text{O}_2^{\cdot-}$, e^- , and h^+ were all trapped by IPA, p-BQ, AgNO_3 , and AO, respectively. As shown in Fig. 12, the degradation rate of RO-16 reduced when any radical scavenger was added, showing that each of the four active species had a particular effect on the photodegradation. AgNO_3

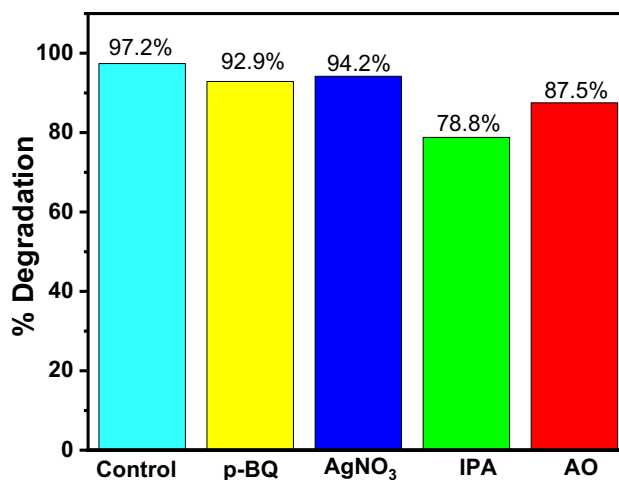


Fig. 12 Effect of some scavengers on the photocatalytic degradation of RO-16 dye over the TCN-15 catalyst dose under visible light irradiation

and p-BQ additions had less impact on the photocatalytic degradation of RO-16, suggesting that e^- and $\text{O}_2^{\cdot-}$ played only minor involvement in the system (Sanakousar et al. 2022a). However, the rate of degradation of RO-16 significantly lowered when the h^+ and $\cdot\text{OH}$ in the system were captured by AO and IPA, respectively. The degradation rate of RO-16 decreased to 78.8% and 87.5%, respectively, after trapping $\cdot\text{OH}$ and h^+ , suggesting that $\cdot\text{OH}$ and h^+ were the primary reactive species for the RO-16 degradation in the TCN-15 composite. Figure 12 represents the role of various active species in photodegradation (Guo et al. 2020).

Mechanism of photocatalytic degradation

The mechanism for the degradation of dyes by the TCN-15 composite has been presented in Fig. 13. When the TCN-15 composite is irradiated with visible light, photoinduced electrons in the conduction band of g- C_3N_4 transfer to the conduction band of TiO_2 while the holes migrate to the valence band of g- C_3N_4 . Resultantly, the recombination of photoinduced charge carriers is prevented. The photoelectrons in the conduction band of TiO_2 undergo a reaction with the molecular O_2 to yield $\text{O}_2^{\cdot-}$ which oxidizes the dyes. The $\text{O}_2^{\cdot-}$ undergoes a reaction with water and produces $\text{HO}^{\cdot-}$ radicals. At the same time, the photoinduced holes (h^+) in the valence band of g- C_3N_4 undergo a reaction with the H_2O yield HO^{\cdot} radicals. The HO^{\cdot} and $\text{O}_2^{\cdot-}$ radicals being strong oxidizing agents degrade the dye molecules into nontoxic end products such as H_2O and CO_2 . Furthermore, the degradation efficiency depends on the absorption ability of visible light, the partition of the charge carriers, and the surface area of the photocatalyst (Sanakousar et al. 2021).

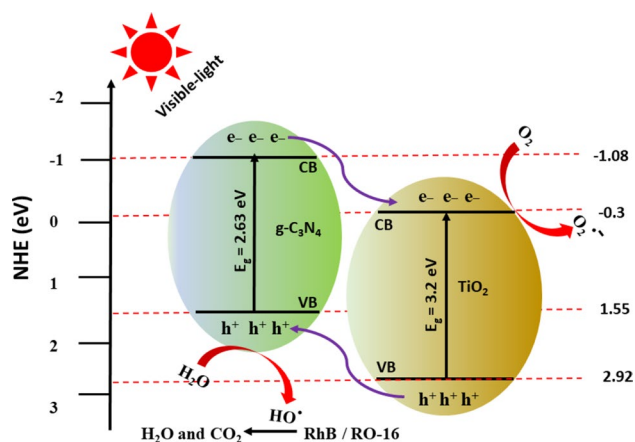


Fig. 13 Mechanism of catalytic degradation of RO-16 dye

Conclusion

In this study, different TCN semiconductors were successfully synthesized and analyzed by advanced techniques. The degrading efficiency of pure $g\text{-C}_3\text{N}_4$, TiO_2 , and all TCN semiconductors was studied against RhB and RO-16 degradation in aqueous media. The TCN-15 composite has shown higher degrading efficiency for both RhB and RO-16 dyes under visible light. The characterization results revealed that the TCN-15 has a large BET surface area and wider visible light response range compared with other composites. The purity of the synthesized composite was analyzed by XRD analysis. The photocatalytic degradation efficiencies were 89.62% and 97.20% for RhB and RO-16, respectively, at optimal conditions such as a catalyst dose (0.07 g), dye concentration (50 ppm), and temperature (50 °C) at neutral pH in 90 min under visible light irradiation. The mechanism for the higher degrading efficiency of the TCN-15 composite has also been proposed. The TCN-15 composite has shown excellent reusability even after five cycles for the degradation of RO-16 dye under exposure to visible light which makes it a promising candidate for commercial-scale environmental applications.

Author contribution Asma A. Alothman: experimental work. Asif Ayub: management of the entire project. Safa K. Hachim: physical studies and data interpretation. Borhan Mustafa Mohammed: transient current studies and proof reading. Farhat Hussain: optical studies and interpretation. Muhammad Altaf: literature search and data analysis. Zainab Jawad Kadhim: SEM and XRD analysis. Holya A. Lafta: write up the reaming manuscript. Yasir S. Alnassar: critical analysis and validation. Marwah A. Shams: critical analysis. Nada A. Almuhou: critical analysis. Mohamed Ouladsmame: critical analysis. Mika Sil-lanpaa: formal analysis.

Funding The authors gratefully acknowledge the financial support from the Researchers Supporting Project Number (RSP-2021/243) King Saud University, Riyadh, Saudi Arabia.

Data availability The datasets used and analyzed during the study are available from the corresponding author upon reasonable request.

Declarations

Ethical approval Not applicable.

Consent to participate Not applicable.

Consent for publication Not applicable.

Competing interests The authors declare no competing interests.

References

- Adeel M, Saeed M, Khan I et al (2021) Synthesis and characterization of Co-ZnO and evaluation of its photocatalytic activity for photo-degradation of methyl orange. *ACS Omega* 6:1426–1435. <https://doi.org/10.1021/acsomega.0c05092>
- Alsalmeh A, Galal AH, El-Sherbeny EF et al (2022) Fabrication of S-scheme $\text{TiO}_2/g\text{-C}_3\text{N}_4$ nanocomposites for generation of hydrogen gas and removal of fluorescein dye. *Diam Relat Mater* 122:108819. <https://doi.org/10.1016/j.diamond.2022.108819>
- Ayub A, Raza ZA (2021) Arsenic removal approaches: a focus on chitosan biosorption to conserve the water sources. *Int J Biol Macromol* 192:1196–1216. <https://doi.org/10.1016/j.ijbiomac.2021.10.050>
- Ayub A, Raza ZA, Majeed MI et al (2020) Development of sustainable magnetic chitosan biosorbent beads for kinetic remediation of arsenic contaminated water. *Int J Biol Macromol* 163:603–617. <https://doi.org/10.1016/j.ijbiomac.2020.06.287>
- Ayub A, Srithilat K, Fatima I et al (2022) Arsenic in drinking water: overview of removal strategies and role of chitosan biosorbent for its remediation. *Environ Sci Pollut Res* 29:64312–64344. <https://doi.org/10.1007/s11356-022-21988-z>
- Camposeco R, Zanella R (2022) Catalytic behavior of gold nanoparticles supported on a $\text{TiO}_2\text{-Al}_2\text{O}_3$ mixed oxide for CO oxidation at low temperature. *Environ Sci Pollut Res* 29:76992–77006. <https://doi.org/10.1007/s11356-022-21076-2>
- de Assis MLM, Junior ED, de Almeida JMF et al (2021) Photocatalytic degradation of Novacron blue and Novacron yellow textile dyes by the $\text{TiO}_2/\text{palygorskite}$ nanocomposite. *Environ Sci Pollut Res* 28:64440–64460. <https://doi.org/10.1007/s11356-021-15519-5>
- Gao B, Wang J, Dou M et al (2020) Enhanced photocatalytic removal of amoxicillin with $\text{Ag}/\text{TiO}_2/\text{mesoporous } g\text{-C}_3\text{N}_4$ under visible light: property and mechanistic studies. *Environ Sci Pollut Res* 27:7025–7039. <https://doi.org/10.1007/s11356-019-07112-8>
- Girish YR, Udayabhanu AG et al (2022) Facile and rapid synthesis of solar-driven $\text{TiO}_2/g\text{-C}_3\text{N}_4$ heterostructure photocatalysts for enhanced photocatalytic activity. *J Sci-Adv Mater Dev* 7:100419. <https://doi.org/10.1016/j.jsamd.2022.100419>
- Guo X, Duan J, Li C et al (2020) Fabrication of $g\text{-C}_3\text{N}_4/\text{TiO}_2$ photocatalysts with a special bilayer structure for visible light photocatalytic application. *Colloids Surf a: Physicochem Eng Asp* 599:124931. <https://doi.org/10.1016/j.colsurfa.2020.124931>
- Jeyaraja S, Palanivel S, Palanimuthu K, Munusamy C (2022) Phycocyanin from *Spirulina platensis* bio-mimics quantum dots photocatalytic activity: a novel approach for dye degradation. *Environ Sci Pollut Res* 29:68280–68292. <https://doi.org/10.1007/s11356-022-20563-w>
- Kholikov B, Hussain J, Zeng H (2021) Gold modified $\text{TiO}_2/g\text{-C}_3\text{N}_4$ for enhanced photocatalytic activities to evolved H_2 fuel. *Inorg*

- Chem Commun 131:108787. <https://doi.org/10.1016/J.INOCHE.2021.108787>
- Kotkar SN, Prasad S, Gadekar GP, Rewatkar SB (2022) Auto combustion synthesis of ZnO for degradation of organic dye under natural solar light with bactericidal activity. *Inorg Chem Commun* 144:109830. <https://doi.org/10.1016/j.inoche.2022.109830>
- Kumar OP, Ahmad M, Nazir MA et al (2022) Strategic combination of metal–organic frameworks and C₃N₄ for expeditious photocatalytic degradation of dye pollutants. *Environ Sci Pollut Res* 29:35300–35313. <https://doi.org/10.1007/s11356-021-17366-w>
- Liu W, Wang Y, Qi K et al (2022) Broad spectral response Z-scheme three-dimensional ordered macroporous carbon quantum dots/TiO₂/g-C₃N₄ composite for boosting photocatalysis. *Langmuir* 38:4839–4847. <https://doi.org/10.1021/acs.langmuir.1c03483>
- Ma L, Wang G, Jiang C et al (2018) Synthesis of core-shell TiO₂@g-C₃N₄ hollow microspheres for efficient photocatalytic degradation of rhodamine B under visible light. *Appl Surf Sci* 430:263–272. <https://doi.org/10.1016/j.apsusc.2017.07.282>
- Mehregan S, Hayati F, Mehregan M et al (2022) Exploring the visible light-assisted conversion of CO₂ into methane and methanol, using direct Z-scheme TiO₂@g-C₃N₄ nanosheets: synthesis and photocatalytic performance. *Environ Sci Pollut Res* 29:74951–74966. <https://doi.org/10.1007/S11356-022-21048-6/FIGURES/9>
- Moustafa HM, Mahmoud MS, Nassar MM (2022) Kinetic analysis of p-rGO/n-TiO₂ nanocomposite generated by hydrothermal technique for simultaneous photocatalytic water splitting and degradation of methylene blue dye. *Environ Sci Pollut Res*. <https://doi.org/10.1007/s11356-022-23430-w>
- Pattanayak DS, Pal D, Mishra J et al (2022) Doped graphitic carbon nitride (g-C₃N₄) catalysts for efficient photodegradation of tetracycline antibiotics in aquatic environments. *Environ Sci Pollut Res*. <https://doi.org/10.1007/s11356-022-19766-y>
- Raziq F, Li C, Humayun M et al (2015) Synthesis of TiO₂/g-C₃N₄ nanocomposites as efficient photocatalysts dependent on the enhanced photogenerated charge separation. *Mater Res Bull* 70:494–499. <https://doi.org/10.1016/J.MATERRESBULL.2015.05.018>
- Saeed M, Muneer M, Haqul A, Akram N (2022) Photocatalysis: an effective tool for photodegradation of dyes—a review. *Environ Sci Pollut Res* 29:293–311. <https://doi.org/10.1007/s11356-021-16389-7>
- Sanakousar MF, Vidyasagar CC, Jiménez-Pérez VM et al (2021) Efficient photocatalytic degradation of crystal violet dye and electrochemical performance of modified MWCNTs/Cd-ZnO nanoparticles with quantum chemical calculations. *J. Hazard. Mater Adv* 2:100004. <https://doi.org/10.1016/j.hazadv.2021.100004>
- Sanakousar FM, Vidyasagar C, Jiménez-Pérez VM, Prakash K (2022a) Recent progress on visible-light-driven metal and non-metal doped ZnO nanostructures for photocatalytic degradation of organic pollutants. *Mater Sci Semicond Process* 140:106390. <https://doi.org/10.1016/j.mssp.2021.106390>
- Sanakousar MF, Vidyasagar CC, Jiménez-Pérez VM et al (2022b) Mechanistic insight into the photocatalytic degradation of organic pollutants and electrochemical behavior of modified MWCNTs/Cu–Co₃O₄ nanocomposites. *React Chem Eng* 7:1847–1872. <https://doi.org/10.1039/D2RE00117A>
- Sun EC, Di WH, Zhang S et al (2022) Adsorption coupling photocatalytic removal of gaseous n-hexane by phosphorus-doped g-C₃N₄/TiO₂/Zn(OAc)₂-ACF composites. *Environ Sci Pollut Res*. <https://doi.org/10.1007/s11356-022-22382-5>
- Tara N, Iqbal M, Habib FE et al (2021) Investigating degradation metabolites and underlying pathway of azo dye “Reactive Black 5” in bioaugmented floating treatment wetlands. *Environ Sci Pollut Res* 28:65229–65242. <https://doi.org/10.1007/s11356-021-15130-8>
- Waghchaure RH, Adole VA, Jagdale BS (2022) Photocatalytic degradation of methylene blue, rhodamine B, methyl orange and Eriochrome black T dyes by modified ZnO nanocatalysts: a concise review. *Inorg Chem Commun* 143:109764. <https://doi.org/10.1016/J.INOCHE.2022.109764>
- Wang P, Guo X, Rao L et al (2018) A weak-light-responsive TiO₂/g-C₃N₄ composite film: photocatalytic activity under low-intensity light irradiation. *Environ Sci Pollut Res* 25:20206–20216. <https://doi.org/10.1007/S11356-018-2201-1/FIGURES/11>
- Wang G, Li Y, Dai J, Deng N (2022) Highly efficient photocatalytic oxidation of antibiotic ciprofloxacin using TiO₂@g-C₃N₄@biochar composite. *Environ Sci Pollut Res* 29:48522–48538. <https://doi.org/10.1007/S11356-022-19269-W/FIGURES/10>
- Yu H, Zhang M, Lv J et al (2022) Fabrication of a stable light-activated and p/n type AgVO₃/V₂O₅-TiO₂ heterojunction for pollutants removal and photoelectrochemical water splitting. *J Alloys Compd* 894:162500. <https://doi.org/10.1016/J.JALLCOM.2021.162500>
- Zada A, Qu Y, Ali S et al (2018) Improved visible-light activities for degrading pollutants on TiO₂/g-C₃N₄ nanocomposites by decorating SPR Au nanoparticles and 2,4-dichlorophenol decomposition path. *J Hazard Mater* 342:715–723. <https://doi.org/10.1016/J.JHAZMAT.2017.09.005>
- Zhang M, Han N, Fei Y et al (2021) TiO₂/g-C₃N₄ photocatalyst for the purification of potassium butyl xanthate in mineral processing wastewater. *J Environ Manage* 297:113311. <https://doi.org/10.1016/J.JENVMAN.2021.113311>

Publisher's note Springer Nature remains neutral with regard to jurisdictional claims in published maps and institutional affiliations.

Springer Nature or its licensor (e.g. a society or other partner) holds exclusive rights to this article under a publishing agreement with the author(s) or other rightsholder(s); author self-archiving of the accepted manuscript version of this article is solely governed by the terms of such publishing agreement and applicable law.